Anharmonicity and atomic distribution of SnTe and PbTe thermoelectrics

C. W. Li, J. Ma, H. B. Cao, A. F. May, D. L. Abernathy, G. Ehlers, C. Hoffmann, X. Wang, T. Hong, A. Huq, O. Gourdon, and O. Delaire

Phys. Rev. B **90**, 214303 — Published 29 December 2014

DOI: 10.1103/PhysRevB.90.214303

Anharmonicity and Atomic Distribution of SnTe and PbTe Thermoelectrics

C.W. Li,[1,*] J. Ma,[2] H.B. Cao,[2] A.F. May,[1] D.L. Abernathy,[2] G. Ehlers,[2] C. Hoffmann,[3] X. Wang,[3] T. Hong,[2] A. Huq,[3] O. Gourdon,[4] and O. Delaire[1]

[1] *Materials Science and Technology Division, Oak Ridge National Laboratory, Oak Ridge, Tennessee, 37831*
[2] *Quantum Condensed Matter Division, Oak Ridge National Laboratory, Oak Ridge, Tennessee, 37831*
[3] *Chemical and Engineering Materials Division, Oak Ridge National Laboratory, Oak Ridge, Tennessee, 37831*
[4] *Lujan Center, Los Alamos National Laboratory, Los Alamos, New Mexico, 87545*

The structure and lattice dynamics of rock-salt thermoelectric materials SnTe and PbTe are investigated with single crystal and powder neutron diffraction, inelastic neutron scattering (INS), and first-principles simulations. Our first-principles calculations of the radial distribution function (RDF) in both SnTe and PbTe show a clear asymmetry in the first nearest-neighbor (1NN) peak, which increases with temperature, in agreement with recent experimental reports. We show that this peak asymmetry for the 1NN Sn–Te or Pb–Te bond results from large-amplitude anharmonic vibrations (phonons). No atomic off-centering is found in our simulations. In addition, the atomic mean square displacements derived from our diffraction data reveal stiffer bonding at the anion site, in good agreement with the partial phonon densities of states from INS, and first-principles calculations. These results provide clear evidence for large-amplitude anharmonic phonons associated with the resonant bonding leading to the ferroelectric instability.

PACS numbers: 63.20.-e, 63.20.dk, 63.20.Ry, 63.20.D-, 78.70.Nx, 84.60.Rb

I. INTRODUCTION

Understanding phonon dynamics is very important in improving the thermoelectric efficiency. The figure-of-merit for thermoelectric conversion efficiency, zT, can be expressed as $zT = \sigma S^2 T/\kappa$, where S, T, σ, and κ are the Seebeck coefficient, temperature, electrical and thermal conductivities, respectively. Thus, a low thermal conductivity is favorable to good thermoelectric performance. The rock-salt compounds PbTe and SnTe are particularly interesting, with zT values reaching well above unity, in part thanks to low lattice thermal conductivities, $\kappa_{\rm lat} \simeq 2$ W m^{-1} K^{-1} at 300 K in single-crystals.[3–9] Several factors contribute to this low $\kappa_{\rm lat}$, including soft bonds, heavy atomic masses, and strong anharmonicity, which is reflected in the proximity to a ferroelectric lattice instability.[10–16]

The half-filled resonant p–band and the nonlinear Te polarizability in group IV tellurides induce a strong anharmonicity in long-range interatomic potentials.[12,13,16,18–22] These interactions along [100] crystallographic directions cause the transverse optic (TO) phonon branch to dip to low energy at the zone-center. The strong anharmonicity causes this zone-center TO phonon to stiffen markedly as T increases in the cubic paraelectric phase, in a clear departure from a quasi-harmonic lattice,[10,23–27] but in general agreement with the soft-mode picture of the ferroelectric transition.[28,29]

Recently, an asymmetry of peaks was reported in the pair-distribution-function (PDF) or radial distribution function (RDF) of PbTe, PbS, and SnTe, which was interpreted in terms of atomic off-centerings increasing with temperature.[1,2,11,30] However, it is important to note that these x-ray PDF/RDF measurements did not filter out the phonon contribution to the scattered intensity, or thermal diffusive scattering (TDS). In addition, the interpretation of PDF/RDF asymmetry in terms of atomic off-centerings was put in question by molecular dynamics simulations, which reproduced the asymmetry in the measurements, but found no time-averaged off-centering on a time scale of 12 picosecond or longer.[13,31] In addition, measurements of the local-structure with x-ray absorption fine structure found no off-centerings in PbTe.[32,33] More recently, a high-resolution neutron powder diffraction study showed no evidence for anomalies in the temperature dependence of atomic displacement parameters (ADPs) in PbS and attributed the unusual temperature behaviors reported in Ref. 1,2 to inaccurate thermometry.[34]

The spectra of PbTe exhibits a broad and split peak at the zone center in the temperatures between 200 and 500 K,[10,11] clearly different from a damped harmonic oscillator profile.[35] A similar double-peak feature was also observed in frequency-dependent reflectivity measurements.[36] It had been previously conjectured that this anomaly could be related to proposed atomic off-centerings causing an additional localized optical mode, beyond the dispersions of the rock-salt structure.[1,11] However, our first-principles calculations of the temperature-dependent spectral density functions showed how the double-peak arises from the shape of the anharmonic phonon self-energy, whose imaginary part contains a pronounced peak, owing to nesting of the phonon dispersions.[37] Calculations of the zone-center TO phonon spectral function at zone center in PbTe based on molecular dynamics also reproduced the effect.[31,38] Our measurements and calculations found a less unusual spectral function for the TO mode in SnTe, although its linewidth is also quite broad.[37]

While PbTe is an incipient ferroelectric material, intrinsic SnTe undergoes a displacive ferroelectric phase transition from a high-temperature paraelectric rock salt

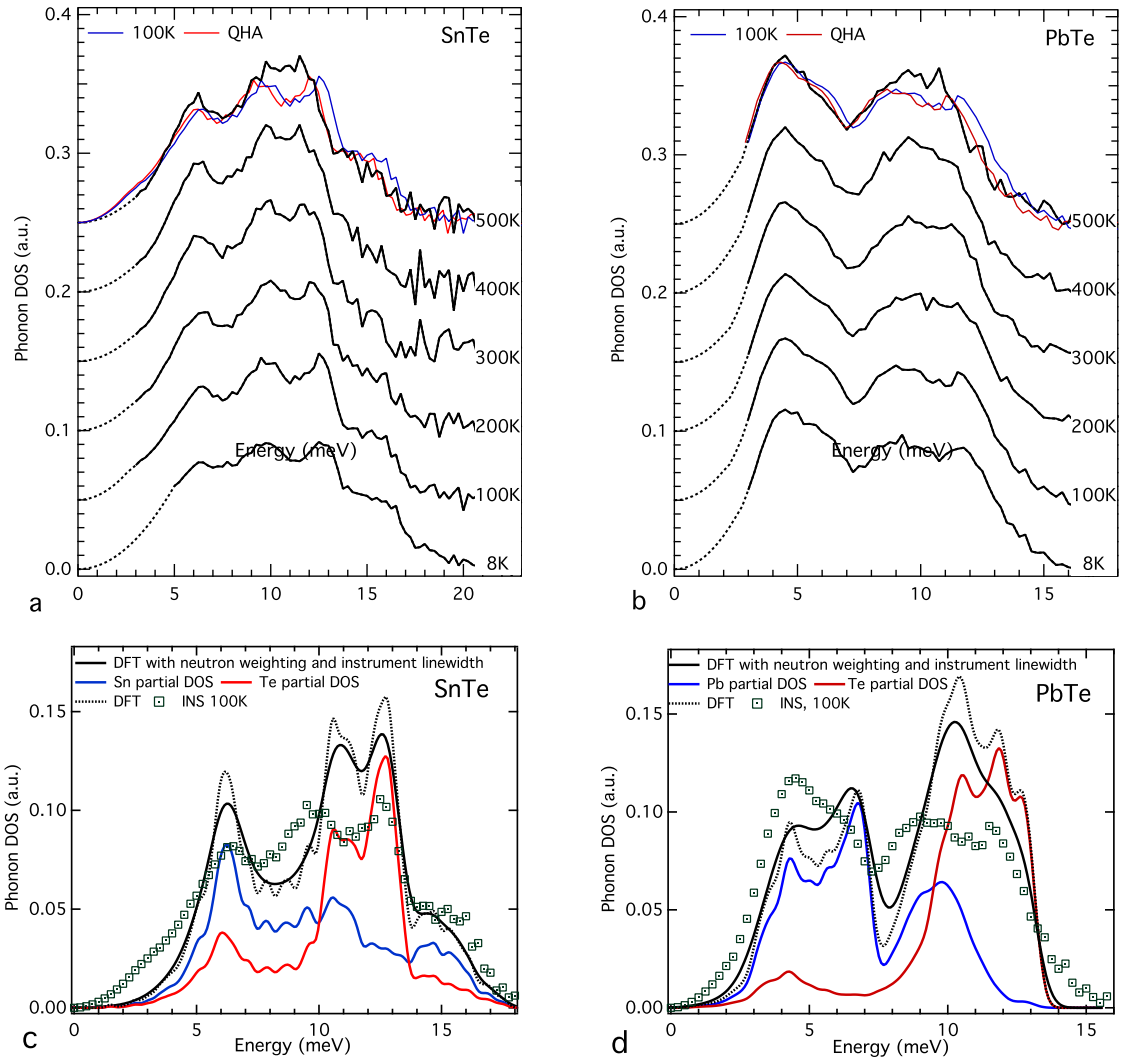

FIG. 1. Phonon density of states of SnTe and PbTe. Generalized phonon DOS of SnTe (a) and PbTe (b) at several temperatures, obtained from powder inelastic neutron scattering on ARCS (incident energy $E_i = 30$ and 25 meV). The curve labeled QHA corresponds to data at 100 K, shifted according to the quasi-harmonic approximation, with the measured volumes at 100 K and 500 K, and an average Grüneisen parameter, $\gamma = 2$ from Ref. 17. Panels (c) and (d) show the total and partial phonon DOS obtained from first-principles calculations. The results after applying neutron weighing and instrument resolution are compared with the neutron DOS at 100 K.

phase to a rhombohedrally distorted ferroelectric phase at a Curie temperature $T_C \lesssim 100$ K, with softening of the TO mode.[29] However, T_C in SnTe is strongly dependent on the introduction of extrinsic carriers, which arises from a slight off-stoichiometry.[24] Samples of SnTe synthesized by solid-state reaction are commonly found to exhibit a small Sn-deficiency, owing to slightly incongruent melting of the rock-salt phase.[39] The transition temperature is about 100K for hole densities below 10^{20} cm^{-3}, but decreases at higher concentration.[40] In ferroelectric SnTe, the dielectric dipole moment arises from an offset of the cation and anion sub-lattices along the cubic $\langle 111 \rangle$ direction, combined with a shortening of the cubic body diagonal.[24] The ferroelectric distortion matches the displacement pattern (eigenvector) of the transverse-optic (TO) phonon at the zone center (Γ), and the transition has early been interpreted in terms of the soft-mode theory of ferroelectricity initially proposed by Cochran.[28,29]

In this study, the phonon DOS of SnTe and PbTe were measured at a series of temperatures with INS. In addition, the atomic mean square displacements were measured with neutron diffraction, on both single-crystalline and powder samples. The combination of these measurements provides a detailed view of the phonon dynamics and anharmonicity. First-principles lattice dynamics and molecular dynamics simulations were performed, and showed good agreement with the measured quantities, in addition to reproducing the asymmetry of the 1NN peak

in the radial distribution function reported in Refs. 1,2.

II. EXPERIMENTS

Single crystals of SnTe and PbTe were grown by a modified Bridgman technique, and characterized with x-ray diffraction and transport measurements. Samples from the same growth were used for the measurements and characterization. For powder neutron diffraction and inelastic scattering phonon DOS measurements, some single crystals were ground into fine powders. The carrier concentration determined from Hall measurements was $n_h \simeq 6.5 \pm 1.5 \times 10^{20}\,\mathrm{h/cm^3}$ in SnTe crystals, and $n_e \simeq 1.7 \times 10^{17}\,\mathrm{e/cm^3}$ in PbTe crystals. The low temperature ferroelectric distortion of SnTe is very small[24] and we could not resolve any splitting of Bragg peaks with either powder or single-crystal neutron diffraction. However, the resistivity measurements on our SnTe crystals showed an anomaly characteristic of the ferroelectric transition at $T_\mathrm{C} \simeq 42\,\mathrm{K}$.[42] This transition temperature is consistent with expectations for this carrier density, based on Raman measurements, transport characterization, and diffraction peak intensities.[24,43] On the other hand, PbTe at the present carrier concentration remains incipient ferroelectric, with an extrapolated $T_\mathrm{C} \simeq -60\,\mathrm{K}$.[24]

The phonon DOS measurements were performed on the powders with the ARCS time-of-flight neutron spectrometer at the Spallation Neutron Source (SNS).[44] The samples were measured at T = 8, 100, 200, 300, 400, and 500 K, using an incident neutron energy of 30 or 25 meV for SnTe and PbTe, respectively. ARCS has an energy-dependent energy resolution that varies from about 4% at the elastic line to 1% at the highest energy transfer. The signal from the empty aluminum sample holder was measured in identical conditions, and subtracted from the data. The time-of-flight data were reduced with MANTID[45] to produce the powder-averaged dynamical structure factor, $S(Q,E)$, as function of energy transfer E and momentum transfer magnitude Q. From this $S(Q,E)$, the generalized (neutron weighted) phonon DOS was obtained by applying corrections for thermal occupation, as well as multiphonon and multiple scattering with incoherent scattering approximation.[46] The results for the phonon DOS are shown in Fig. 1.

Powder and single-crystal neutron diffraction measurements were performed with POWGEN and TOPAZ at SNS and HB-3A at the High-Flux Isotope Reactor (HFIR). In the POWGEN powder diffraction measurements, two frames corresponding to bands of neutron wavelengths centered around 0.533 and 1.59 Å were used, to cover a large range of momentum transfers. The powder was loaded in a vanadium can and mounted in either a closed-cycle refrigerator or a furnace for measurements from 100 to 450 K. For single-crystal diffraction measurements on TOPAZ and HB-3A, samples were cut into cubes about $2\times2\times2\,\mathrm{mm^3}$ and $3\times3\times3\,\mathrm{mm^3}$, respectively, with the corners rounded. After cutting and shaping, all samples were sealed in quartz tubes and annealed at 600 K for three days. On TOPAZ, the crystals were mounted in a cold nitrogen flow and measured using neutron wavelengths between 0.3 and 3.5 Å at 100, 200, 300, 350, 400, and 450 K. On HB-3A, the crystals were mounted in a high-temperature closed-cycle refrigerator and measured using neutrons wavelength of 1.003 Å at 5, 50, 100, 150, 200, 250, 300, and 450 K. The integrated peak intensities were analyzed with the software *Fullprof*[47], and atomic mean square displacements (MSD) were obtained from the Rietveld refinements. Typical refinement factors at 300 K were listed in Tab. I. The results for MSD values as function of temperature are shown in Fig. 2. It should be noted that our SnTe crystals are in low symmetry phase at $T < 42$ K.

TABLE I. Diffraction refinement parameters at 300 K.

	HB-3A				TOPAZ			
	SnTe		PbTe		SnTe		PbTe	
RF^2w	3.60		6.19		6.8		6.0	
RF	1.83		3.07		3.6		2.7	
χ^2	0.569		3.00		2.83		4.02	
$\langle u^2\rangle$	Sn	Te	Pb	Te	Sn	Te	Pb	Te
(10^{-2}Å^2)	1.919	1.467	2.025	1.528	2.269	1.521	2.369	1.705

Single crystal inelastic neutron scattering (INS) measurements were performed with the CNCS cold neutron time-of-flight spectrometer at the SNS[48] and the CTAX cold triple-axis spectrometer at HFIR. CNCS measurements were performed with incident energies $E_i = 12$ and 25 meV (the energy resolution at elastic line is 0.5 meV), and at two different temperatures (50 and 300 K). The crystals were oriented with the $[\bar{1}10]$ axis vertical, and data were collected for multiple rotations around this direction, over a wide range of angles. The data were subsequently combined to generate the four-dimensional scattering function, $S(\mathbf{Q},E)$, using standard software,[45,49] and then "sliced" along selected $\mathbf{Q}$-directions to produce two-dimensional views, some of which are shown in Fig. 3 for SnTe. Data from lower incident energy provides better resolution, but limited $\mathbf{Q}$ and E coverage. Acoustic phonons of SnTe near the Γ-point were measured with CTAX, using PG002 monochromator and analyzer, with a constant final energy $E_f = 5.0$ meV, and collimation settings of 48′-40′-40′-120′. The spectra for longitudinal acoustic phonons were refined to extract the phonon energy and linewidth by computing the convolution of the CTAX instrument resolution function with a Lorenzian function as implemented in the single mode approximation in Reslib package.[50] Figure 4 shows the results from fitting the constant-$\mathbf{Q}$ cuts from both CTAX and CNCS.

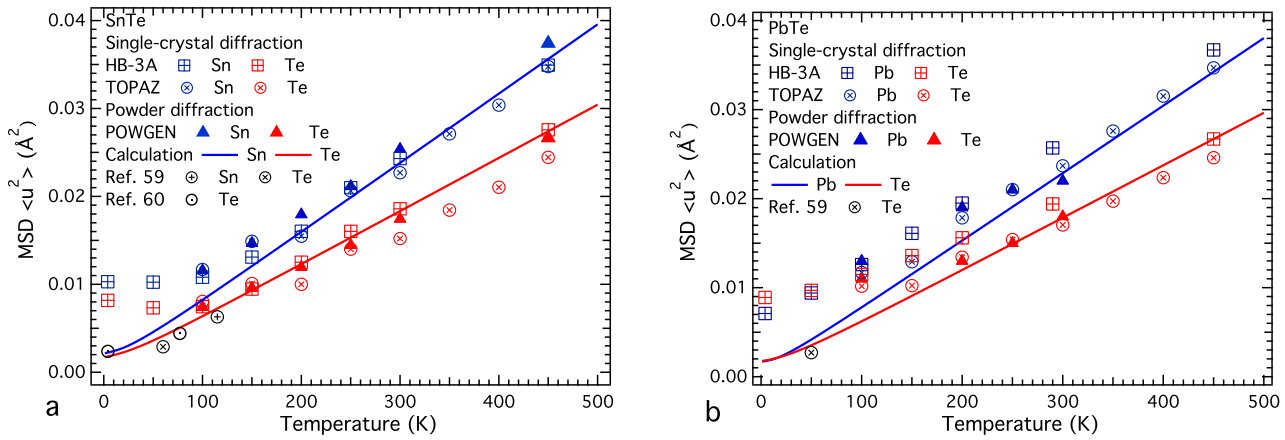

FIG. 2. Mean square atomic displacements for SnTe (a) and PbTe (b), measured with neutron diffraction (markers), and calculated (lines) from the theoretical partial phonon DOS curves of Fig. 1. Open color markers correspond to MSD values measured with neutron single crystal diffraction (HB-3A and TOPAZ), while filled color markers are values from powder diffraction (POWGEN). Black markers correspond to values in the literature. Blue lines and markers correspond to Sn or Pb, and red to Te. The vibration amplitudes of the cations are systematically larger than those of Te anions.

III. FIRST-PRINCIPLES SIMULATIONS

There has been considerable interest in calculating the phonon modes in SnTe and PbTe.[51–53] While some of these calculations reproduced the soft TO phonon modes and the lattice instability at low temperature, they offered only limited insight about the anharmonicity, except for a recent study by Lee *et al.*[16] In order to capture the full extent of anharmonicity on the phonons at finite temperature, ab-initio Born-Oppenheimer molecular dynamics (MD) simulations were performed at 100, 300, and 600 K with VASP[54–56]. Calculations used the generalized gradient approximation (PBE) and projector augmented wave (PAW AM05) pseudopotentials with an energy cutoff of 300 meV. The MD simulations of a $3\times3\times3$ (216 atoms) supercell were first carried out with Γ–point only Brillouin zone integration for more than 20 ps after equilibration with a time step of 2 fs, and the temperature was controlled with a Nosé thermostat. Subsequently, 30 uncorrelated steps from the MD trajectories were re-calculated with a $3\times3\times3$ electronic k−point grid. The convergence was tested against the size of the supercell, cutoff energy, simulation length, and cutoff distance of the force constants. The translational invariance was imposed. Harmonic, third, and fourth order anharmonic terms in interatomic force-constants were obtained by fitting an effective anharmonic hamiltonian to these atomic configurations and corresponding forces following the temperature-dependent effective potential (TDEP) methodology, as developed by Hellman *et al.*[57] The phonon DOS and dispersions were calculated using renormalized harmonic force constants at 300 K (from the TDEP procedure). The total and atom-projected (partial) phonon DOS computed for SnTe and PbTe using tetrahedron-integration are shown in Fig. 1a,b. The phonon dispersions of SnTe are shown in Fig. 3 (last column). First principles frozen phonon calculations show that, at their respective relaxed lattice parameters, SnTe has a double-well potential with two minima offset from the rock salt position, while PbTe shows a single minimum centered at the equilibrium configuration.[37] This is in good agreement with the experimental observation that stoichiometric SnTe is ferroelectric while PbTe is paraelectric down to 0 K, and thus SnTe is closer to the ferroelectric instability than PbTe. The TDEP method at the calculated temperatures yields stable phonons, and reproduces the experimental observation of stabilization of the soft TO mode with increasing T.

In order to compare with the INS measurements, the dynamical structure factor was computed from the first-principles phonon dispersions and polarization vectors (ϵ_{ds}), as follows:[58]

$$S(\mathbf{Q},E) \propto \sum_s \sum_\tau \frac{1}{E_s} \left| \sum_d \frac{\bar{b}_d}{\sqrt{M_d}} e^{(-W_d + i\,\mathbf{Q}\cdot\mathbf{r}_d)} (\mathbf{Q}\cdot\epsilon_{ds}) \right|^2 \times \langle n_s+1\rangle\, \delta(E-E_s)\, \delta(\mathbf{Q}-\mathbf{q}-\tau)\ , \qquad (1)$$

where s, τ, and d denotes the branch index, reciprocal lattice vector, and atom index in the unit cell, respectively, and $\bar{b}_d$, $\mathbf{r}_d$, and M_d are the coherent neutron scattering length, position, and atomic mass for atom d. The Debye-Waller factor, W_d, was calculated assuming the MSDs are isotropic and using their values from the simulation as described earlier. The result was convoluted with a 4-dimensional gaussian instrument resolution function for CNCS, $R(\mathbf{Q},E)$. A constant $\mathbf{Q}$ resolution, of comparable width as the bin sizes of $S(\mathbf{Q},E)$ integration and a known, energy-dependent energy resolution were used.[48] The results are in good agreement with the INS measurement, as can be seen in Fig. 3, validating the finite-temperature phonon dispersion calculations.

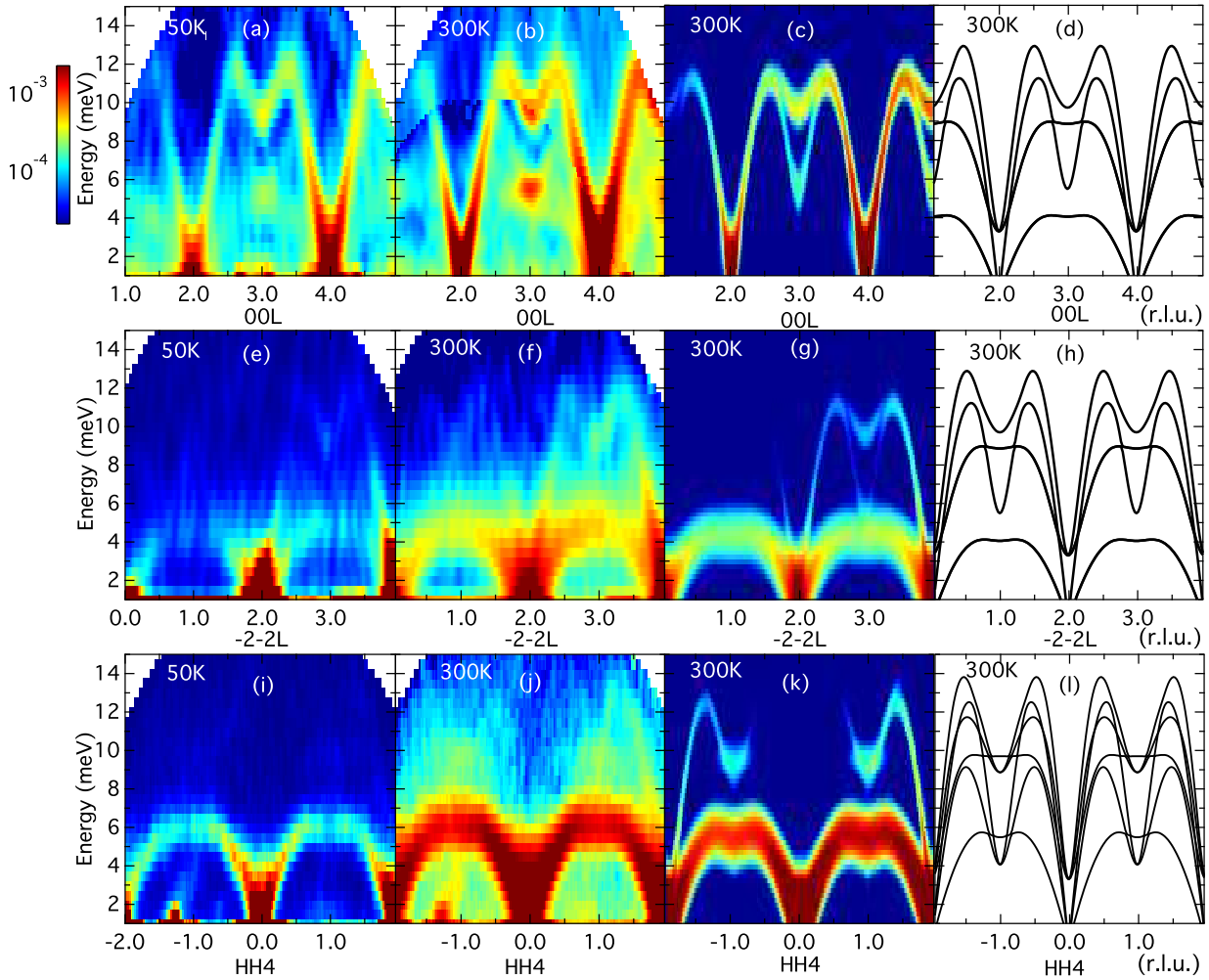

FIG. 3. SnTe: slices of dynamical structure factor, $S(Q,E)$ along [0,0,L] direction measured on CNCS at (a) 50 and (b) 300 K, compared with first-principles simulations (c) and phonon dispersion (d). $S(Q,E)$ along [-2,-2,L] direction showing same phonon dispersion branches, but stronger transverse acoustic phonons, owing to polarization factor, $(\mathbf{Q}\cdot\epsilon_{ds})$ in Eq. 1, measured at (e) 50 and (f) 300 K, compared with first-principles simulations (g) and phonon dispersion (h). $S(Q,E)$ along [H,H,4] direction measured on CNCS at (i) 50 and (j) 300 K, compared with first-principles simulations (k) and phonon calculation (l). (Intensities are integrated over $\pm 0.1\, r.l.u.$ along $[0,0,1]$ and $[1,\overline{1},0]$ directions, and plotted on a logarithmic-scale.)

IV. LATTICE DYNAMICS

Phonon dispersions of SnTe were measured at 100 K by Cowley *et al.*,[51] but that study did not investigate the temperature dependence. While Pawley reported the temperature dependence of the TO mode from 6 to 300 K, their sample remained cubic at all temperatures, probably as a result of a high hole concentration.[29] The partial phonon densities of states (DOS) of Sn and Te were previously measured in rock-salt SnTe at 60 K using nuclear-resonant inelastic x-ray scattering, and it was found that the phonons are softer than similar materials in rhombohedral phase.[59] In addition, lattice dynamics study of SnTe using Mössbauer spectroscopy suggested the existence of low-temperature anharmonicity.[60] Our more detailed measurements of the temperature-dependent phonon dispersions and DOS provide further information about the phonon dynamics and anharmonicity, and also enable to clarify the origin of asymmetric PDF/RDF peaks observed in diffraction experiments.

Generalized phonon DOS curves from inelastic neutron scattering are "neutron-weighted" because phonon scattering by the different elements occurs with different efficiencies, proportional to their total neutron scattering cross section divided by atomic mass, $\sigma_{\rm scat}/M$. For comparison with experimental results, the TDEP calculated phonon partial DOS curves of Sn/Pb and Te were multiplied by $\sigma_{\rm scat}/M$ and summed to give "neutron-weighted" DOS curves. The result was then convoluted

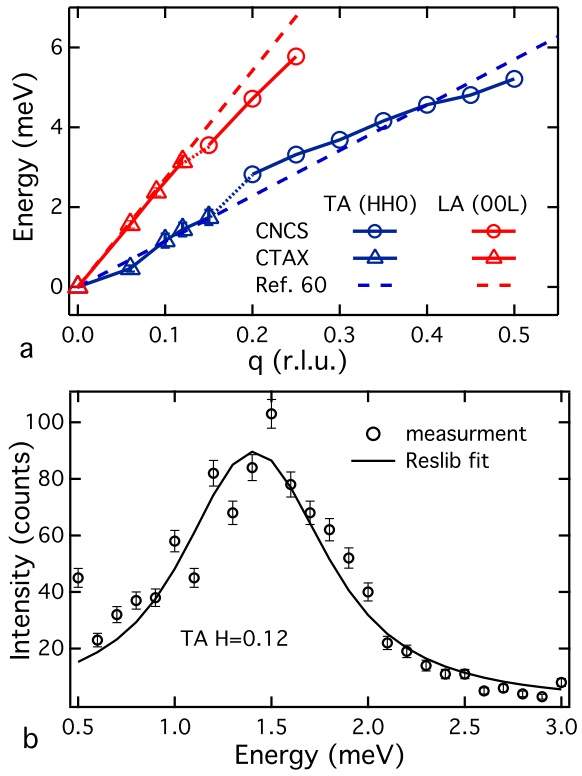

FIG. 4. Longitudinal acoustic phonon dispersion relation and linewidth near zone center, measured near 002 on CTAX and near 004 on CNCS along HH0 and 00L directions at 300K (a). The error bars indicate measured phonon linewidth after instrument resolution correction. The dashed lines show the results from sound velocity measurements.[41] The measurements are resolution limited for CNCS and no resolution is shown. The Reslib fit for the TA mode at q=[0.12, 0.12, 0] is shown in (b).

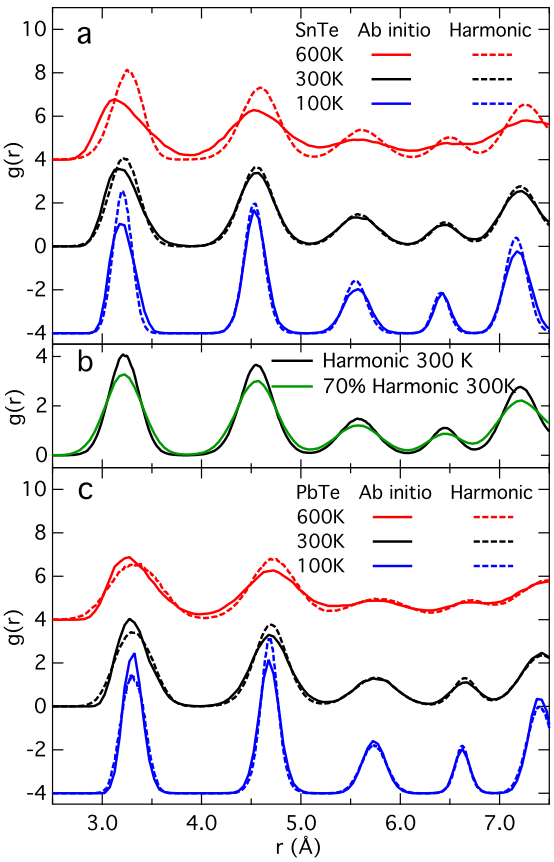

FIG. 5. Radial distribution functions of SnTe (**a**) and PbTe (**c**) calculated from first-principles molecular dynamics and harmonic classical molecular dynamics (using effective harmonic force-constants extracted from the former). Note that full anharmonic calculation results in asymmetric peaks, especially for the 1NN bond, while the harmonic model shows symmetric peaks. In addition, softening the harmonic force-constants by 30% does not induce asymmetry, as shown by the results for SnTe in **b**.

with the energy-dependent instrument resolution function of ARCS to produce an approximate experimental phonon DOS with neutron weighting, as shown in Fig. 1.

We find a fair agreement between this neutron-weighted phonon DOS curve, calculated in the renormalized harmonic approximation with TDEP, and the generalized phonon DOS from powder INS for SnTe and PbTe, as can be seen in Fig. 1. The neutron-weighted phonon DOS agrees well with previous nuclear inelastic scattering measurement of Sn and Te at 115 and 60 K, respectively.[59] However, there are a few differences between INS and calculation. The experimental DOS for SnTe shows a higher intensity near 3∼4 meV at $T = 100\,\mathrm{K}$, which subsides at higher temperatures. This is in agreement with the very soft nature of the zone-center TO phonon mode at 100 K, as a precursor to the ferroelectric phase transition. The experimental DOS for PbTe shows a lesser enhancement at low energy, consistent with the incipient character of the ferroelectric transition in this material ($T_C < 0$). In both materials, there are also some differences in the mid-energy region between 7 and 11 meV, with the measured DOS showing softer and broader phonon modes. According to calculated phonon dispersion relations (Fig. 3) and mode eigenvectors, a large contribution to DOS in this range arises from transverse optical phonons. This discrepancy between the measured DOS and the harmonic calculations is thus consistent with the anharmonicity of the TO branches. This is consistent with the previous results that the low energy phonons are confined to the zone center and have small influence on the phonon DOS. Using the simulated partial phonon DOS, it is possible to correct the neutron weighting from the measured generalized phonon DOS. After performing this correction, we find that the average phonon energies in the de-weighted DOS at 100 K (Fig. 1) are 9.9 and 8.2 meV for SnTe and PbTe, respectively. The Debye temperatures (θ_D)

calculated from the average phonon energy ($\langle E \rangle$) using $k_B\theta_D = \frac{4}{3}\langle E \rangle$, are 115 and 95 K, respectively.

The temperature dependence of the phonon DOS provides insights into the thermal effects on the vibrational energies in the lattice. All DOS curves show three main peaks, which corresponds to the flat portions at the top of phonon dispersions (van Hove singularities). While the lowest peak between 4 and 7 meV is dominated by the top of the transverse acoustic (TA) branches, the other two are mixtures of longitudinal acoustic (LA), transverse optical (TO), and longitudinal optical (LO) branches. For both materials, the peak at intermediate energies (around 9 meV at 100 K) slightly stiffens with increasing T, while the higher-energy peak (around 12 meV at 100 K) significantly softens, leading to these two peaks merging. On the other hand, the low-energy TA peak appears almost unaffected by temperature.

Using an average Grüneisen parameter of 2.0, as calculated from the third-order interatomic force-constants using TDEP method as described in the reference[61], and in agreement with a thermodynamical estimate[17], and using the thermal expansion results from neutron diffraction, it is possible to simulate the effect of lattice dilation with the quasi-harmonic approximation (QHA). The results, for both SnTe and PbTe, shown as red line in Fig. 1, are quite different from the high temperature measurement, indicating a large amount of anharmonicity, especially for the higher energy optical phonons.

We note that for both SnTe and PbTe, there is a spectral separation between the metal and tellurium partial phonon DOS. While this is expected for PbTe because of its large cation/anion mass ratio ($M_{\rm Pb}/M_{\rm Te} = 1.62$), it is unexpected for SnTe since Sn is slightly lighter than Te ($M_{\rm Sn}/M_{\rm Te} = 0.93$). However, this behavior is understood by inspecting the magnitude of the on-site force-constants, which are significantly smaller for the cations than for the anions. This trend is already observed in harmonic-level calculations of the force-constants, and remains valid in finite-temperature TDEP calculations. For example, the on-site force constant on Te (3.0 eV/Å for harmonic model and 2.7 eV/Å for TDEP at 300 K) is larger than the one on Sn (2.2 eV/Å for harmonic model and 2.0 eV/Å for TDEP at 300K). As a result, Te contributes more to the higher energy portion of the DOS than Sn. This may be understood from the bonding states resulting primarily from extended Te p orbitals pointed along $\langle 100 \rangle$.[16]

Further examination of force-constants from TDEP provide important insights about the bonding in these materials. Our calculations find the largest harmonic force-constants between 4NN atoms in SnTe, which correspond to second neighbors along $\langle 100 \rangle$ directions (Sn-Sn and Te-Te: both 0.56 eV/Å^2 at 300K), even larger than the 1NN Sn-Te term, also along $\langle 100 \rangle$ (0.36 eV/Å^2 at 300K). The trend is similar in PbTe (Pb-Pb 4NN: 0.49 eV/Å^2, Te-Te 4NN: 0.52 eV/Å^2, and Pb-Te 1NN: 0.40 eV/Å^2). Even for third-order force constants, the terms involving 4NN atoms are larger than all others, except for the 1NN bonds. In all cases, the harmonic and anharmonic force-constants are strongly anisotropic, with longest-range interactions along $\langle 100 \rangle$ directions. These results are in line with the recent analysis of force-constants by Lee *et al.* in terms of resonant bonding in PbTe and SnTe.[16]

From our SnTe measurements on CTAX, phonon scattering rates were extracted, from which the contribution of acoustic phonons to the lattice thermal conductivity, $\kappa_{\rm lat}$, could be estimated. The contribution of a given phonon mode $(\mathbf{q}, j)$ to the total $\kappa_{\rm lat}$ is: $\kappa_{{\rm latt},\mathbf{q},{\rm j}} = \frac{1}{3} c_{\mathbf{q},j}\, v^2_{\mathbf{q},j}\, \tau_{\mathbf{q},j}$, where $c_{\mathbf{q},j}$ is the mode heat capacity, $v_{\mathbf{q},j} = |\partial\omega_{\mathbf{q},j}/\partial\mathbf{q}|$ is the mode group velocity, and $\tau_{\mathbf{q},j} = \hbar/(2\Gamma_{\mathbf{q},j})$ is the mode lifetime, determined from the measured mode linewidth, $2\Gamma_{\mathbf{q},j}$. From neutron measurements of SnTe, the group velocities are approximately 4.00×10^3 and 1.25×10^3 m/s for the LA mode along $[0,0,L]$ and for the TA mode along $[H,H,0]$, respectively, according to the dispersion slopes shown in Fig. 4. It should be noted that the sound velocities in SnTe depend on the carrier concentration. Ultrasound measurements on a sample with hole concentration of $n_h = 4.5 \times 10^{20}$ h/cm^3, close to the value in our sample, yield velocities of 4120 m/s for LA mode along $[0,0,L]$ and 1220 m/s for TA mode along $[H,H,0]$ polarized in $[0,0,L]$ direction.[41] The phonon linewidths, with instrument contribution subtracted, at 0.1 *r.l.u.* from the zone center, are 0.31 and 0.35 meV for LA and TA modes respectively. These values were obtained from the refinement as mentioned earlier. Using the measured linewidths, the average group velocity of the three modes, and the total lattice heat capacity of SnTe, the estimated contribution from acoustic modes is 2.8 W/(m K) at 300K. This estimate is larger than the value determined by subtracting the electronic component from the total thermal conductivity measurement (2 W/(m K)), especially considering that optical modes are expected to also contribute about 20% of the lattice conductivity.[15] The overestimation is likely associated to our simple extrapolation of linear acoustic dispersions to the entire Brillouin zone.

V. ATOMIC DISTRIBUTIONS

In figure 2, we compare the atomic mean square displacements obtained from diffraction experiments with three different instruments (TOPAZ and HB-3A for single-crystals, and POWGEN for powders). The results from these different measurements agree well overall. The single crystal diffraction measurements provided more accurate intensities of the Bragg peaks, especially for the odd-order peaks in SnTe, which are especially weak due to the small contrast between Sn and Te neutron scattering lengths. As a result, for SnTe we expect more reliable refinement of MSD with single-crystal than powder diffraction. The contrast between Pb and Te is stronger and this was less an issue in PbTe powder mea-

surements.

In the harmonic approximation, the MSD for each crystallographic site and species solely depends on its partial phonon DOS, $g(\omega)$, and atomic mass M, and can be calculated with temperature-dependent phonon occupations:[58]

$$\left\langle u^2_{har} \right\rangle = \frac{3\hbar}{2M} \int \frac{1}{\omega} \coth(\frac{\hbar\omega}{2k_BT}) g(\omega) d\omega \quad . \qquad (2)$$

In Fig. 2, we compare the measured MSD in PbTe and SnTe (markers) with the expected value in the harmonic approximation, based on the partial phonon DOS calculated from first-principles (lines). The results are similar to those at low temperatures in the literature, also calculated from partial phonon DOS[59] for Sn and Te and from Mössbauer[60] for Te, although a direct comparison is not warranted, since carrier concentrations were not reported for samples used in those studies. The calculated and measured MSD are in good agreement above 100 K in both systems. In particular, we do not see any constant offset at high temperatures, which rules out the presence of static displacements. We note that both anions and cations show MSDs that are linear in T at high temperature, with a larger slope for cations. The larger cation MSD was noted in Ref.[59], but no clear origin for the effect was found. Our detailed DFT simulations actually reveal that these large MSD values for cations arise from the weaker on-site force-constants for cations, in good agreement with prior DFT investigations of the bonding and phonons in these materials[13–16,38]. This is in agreement with the equation above, since the weaker cation bonding leads to their softer partial phonon DOS discussed above. On the other hand, below 100 K, the MSDs from diffraction experiments significantly exceed the harmonic prediction (Fig. 2), for both SnTe and PbTe. This behavior is expected because some phonon modes, especially the TO modes near the zone center, have a strongly anharmonic potential energy curves with a flat bottom (or a shallow double-well in the case of SnTe), resulting in larger zero-point motion than expected for harmonic oscillators. Since the strongly anharmonic portion of the soft TO mode is confined to a small reciprocal volume around the zone-center, the soft-mode only contributes a small spectral weight in the phonon DOS, but it can still provide a large MSD. While some residual contribution from the Rietveld refinement procedure cannot be entirely ruled out, we note that there is no systematic offset between the refined ADPs at high temperature and the values computed from Eq. 2. At high temperatures, the good agreement between measured MSDs and the harmonic model is expected, since the entire phonon spectrum is thermally populated, and most of these modes behave harmonically. On the other hand, the steep walls of the TO potential lead to a reduced relative MSD contribution from the soft-mode at high-temperature, especially as it is strongly renormalized[37]. Thus, the proposal that atoms would occupy off-centered positions increasingly deviating from their average crystallographic sites as T increases[1,2,30] is not supported by our data. Instead, we find that the large MSDs, increasing linearly at high T, are predominantly a reflection of large-amplitude thermal vibrations in these softly-bonded materials, in agreement with first-principles simulations. We also note that our results for PbTe are in good agreement with those of Ref.[34] for PbS, adjusted for the heavier overall mass of PbTe.

To understand the asymmetric peaks in PDFs and RDFs reported in the literature[1,11,30], we performed several types of molecular dynamics simulations. Because it is straightforward to convert between PDF and RDF with different normalization, to illustrate the peak asymmetry better, RDF was used for discussion here. First, the RDF was directly calculated from the first-principles molecular dynamics trajectories (the same potentials and supercell as described earlier, $3\times3\times3$ electronic k−point grid, 10 ps at 2 fs time step, $T = 100, 300, 600$ K). Results are shown as solid lines in Fig. 5(a) and (c) for SnTe and PbTe, respectively. For both SnTe and PbTe, these first-principles MD RDFs reproduce the asymmetry of the peaks observed experimentally from x-ray diffraction ("total scattering")[1,2], and also reproduced in previous ab-initio MD simulations[13], and classical MD simulations based on anharmonic interatomic potentials.[31] The distortion of the peaks is obvious for $T \geqslant 300$ K, and can be quantified in terms of the peak skewness, γ, which is defined as the third standardized moment, $\gamma = \mu_3/\sigma^3$, in which μ_3 is the third central moment and σ is the standard deviation. The skewness of the 1NN peak is $\gamma = 0.413$ and 0.379 for SnTe and PbTe at 300 K, respectively. The skewness takes similar values at 600 K, but it is much smaller at 100 K (SnTe: 0.224; PbTe: 0.180). The average MSD of SnTe at 300 K, estimated by the width of the first nearest neighbor peak in RDF, $\langle u^2 \rangle = 0.022$ Å^2, in good agreement with our diffraction measurements.

In order to evaluate the role of anharmonicity in the atomic potential, classical MD simulations on a same supercell were performed with effective harmonic force-constants fitted to the AIMD trajectories, using the TDEP method described earlier. Such renormalized harmonic force-constants were obtained for each AIMD temperature. Because of the low computational cost, the classical MD was performed for 200 ps at 2 fs time step. We note that the resulting T-dependent renormalized harmonic potential was similar whether fits also included third and fourth-order force constants, or only the harmonic components. Harmonic RDFs were then calculated from the resulting harmonic MD trajectories. Strikingly, these harmonic RDFs show almost symmetric peaks at all temperatures (dashed curves in Fig. 5(a) and (c)). The skewness of the 1NN peaks in RDF at 300 K is −0.002 and 0.053 for SnTe and PbTe respectively, close to zero within the statistical uncertainty. This is a strong confirmation that the asymmetry in RDF arises from the anharmonicity in the potential energy surface of these materials. We note that the widths of

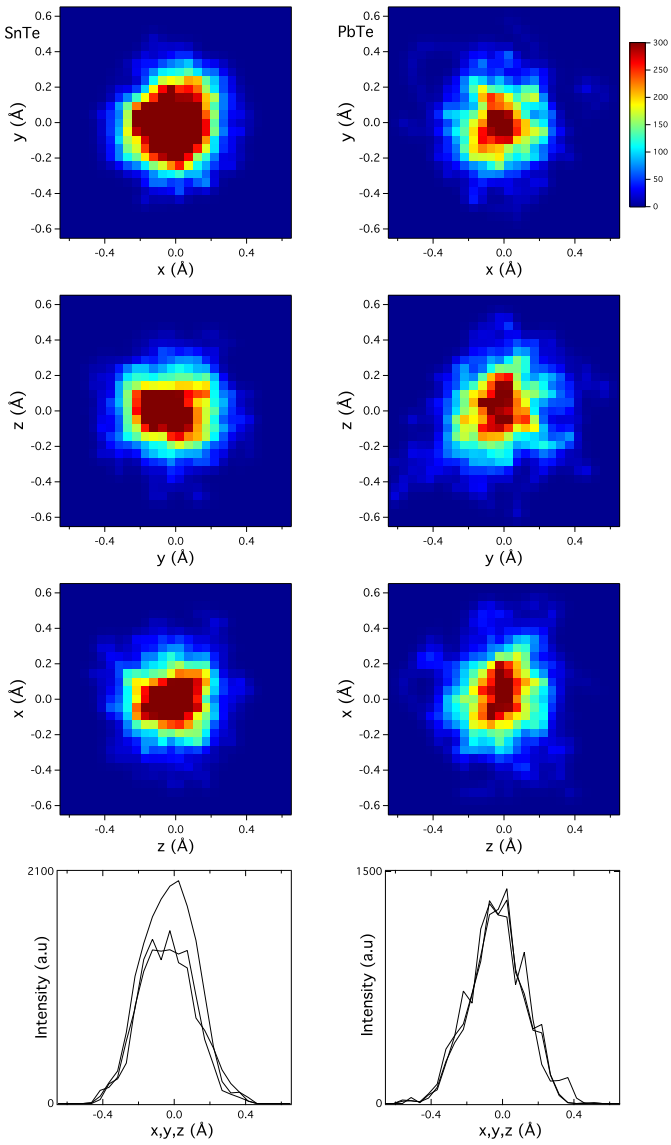

FIG. 6. The probability distribution functions of Sn/Pb atom in SnTe/PbTe, calculated from first-principles molecular dynamics at 300 K show no sign of off-centering. The origin is the average crystallographic position. The integration range along the axis perpendicular to the visualized plane is ±0.1Å. The color scale is linear. For one dimensional cuts, the integration ranges along the two integrated axes are both ±0.1Å.

the peaks in harmonic RDFs are almost the same as in the full anharmonic AIMD calculations. In addition, an harmonic classical MD for SnTe, with its harmonic force-constants reduced by 30%, also resulted in an RDF with symmetric peaks, as illustrated in Fig. 5(b). This indicates that weak force-constants alone are not sufficient to induce asymmetry in the RDF, and that anharmonicity is needed to produce the effect. Furthermore, we investigated the nuclear probability density function of Sn or Pb from the first-principles molecular dynamics trajectory. The results, shown in Fig. 6, confirm the absence of atomic off-centerings in AIMD runs of a couple picoseconds, in agreement with prior simulations.[13]

The asymmetry (skewness) of the 1NN peaks in the first-principles PDF of SnTe and PbTe are similar, with the former being slightly larger. Their temperature dependence is also similar. On the other hand, we have previously shown that the zone-center TO phonon spectral functions of SnTe and PbTe are different. The TO mode spectral function in SnTe does not exhibit the double peak present in PbTe.[37] This leads to the conclusion that the asymmetry of the 1NN PDF peak probes anharmonicity differently than the phonon spectral function. Indeed, we have found that the harmonic, cubic, and quartic interatomic force-constants in SnTe and PbTe have very similar values (similar bonding and anharmonicity), explaining the similar RDFs.[37] On the other hand, the phonon spectral functions computed from the phonon self-energy showed that the anomalous line-shape of the zone-center TO mode in PbTe results from an enhancement of the imaginary part of the self-energy, owing to the opening a large phase-space for three-phonon interactions.[37] We point out that asymmetry in PDF peaks is a good indication of anharmonic interatomic potentials, and could be used to screen materials for strong anharmonicity.

VI. CONCLUSION

The anharmonic lattice dynamics of rock-salt thermoelectric materials SnTe and PbTe were investigated with neutron diffraction, inelastic neutron scattering, and first-principles calculations. The atomic mean square displacements were derived from the diffraction data, and agree well with the values predicted from the partial phonon DOS above 100 K, indicating that there are no atomic off-centerings at these temperatures. This conclusion is confirmed with ab-initio molecular dynamics simulations, which show no off-centering on a time scale of a few picoseconds. Radial distribution functions were calculated from molecular dynamics simulations, both at the level of PAW-PBE ab-initio MD and using effective harmonic force-constants derived from the high-temperature AIMD. The results indicate that the asymmetry of the peaks in the radial distribution function, in particular for the 1NN bond, can be explained by large-amplitude anharmonic thermal vibrations of atoms (i.e. anharmonic phonons).

ACKNOWLEDGMENTS

O.D acknowledges support by the U.S. Department of Energy, Office of Science, Basic Energy Sciences, Materials Sciences and Engineering Division, through the Office of Science Early Career Research Program. C.W.L. and J.M. were supported by the US DOE, Office of Science, Basic Energy Sciences, as part of the S3TEC Energy

Frontier Research Center, DOE Grant DE-SC0001299. Sample synthesis (A.F.M) was supported by the U.S. Department of Energy, Office of Basic Energy Sciences, Materials Sciences and Engineering Division. Modeling of neutron data was developed as part of CAMM, funded by the U.S. Department of Energy, Basic Energy Sciences, Materials Sciences and Engineering Division. The use of Oak Ridge National Laboratory's Spallation Neutron Source and High Flux Isotope Reactor was sponsored by the Scientific User Facilities Division, Office of Basic Energy Sciences, U.S. DOE. This research used resources of the National Energy Research Scientific Computing Center, which is supported by the Office of Science of the U.S. DOE. We thank O. Hellman for providing the TDEP software used in the calculation and B. C. Chakoumakos for helpful discussions.

* lic2@ornl.gov

[1] E. S. Božin, C. D. Malliakas, P. Souvatzis, T. Proffen, N. A. Spaldin, M. G. Kanatzidis, and S. J. L. Billinge, Science **330**, 1660 (2010).
[2] K. R. Knox, E. S. Božin, C. D. Malliakas, M. G. Kanatzidis, and S. J. L. Billinge, Physical Review B **89**, 014102 (2014).
[3] G. J. Snyder and E. S. Toberer, Nature Materials **7**, 105 (2008).
[4] Y. Pei, X. Shi, A. LaLonde, H. Wang, L. Chen, and G. J. Snyder, Nature Materials **473**, 66 (2011).
[5] K. Biswas, J. He, I. D. Blum, C.-I. Wu, T. P. Hogan, D. N. Seidman, V. P. Dravid, and M. G. Kanatzidis, Nature Materials **489**, 414 (2012).
[6] D. Parker, X. Chen, and D. J. Singh, Physical Review Letters **110**, 146601 (2013).
[7] L. Xu, H.-Q. Wang, and J.-C. Zheng, Journal of Electronic Materials **40**, 641 (2011).
[8] G. A. Akhmedova and D. S. Abdinov, International Journal of Thermophysics **45**, 854 (2009).
[9] Q. Zhang, B. Liao, Y. Lan, K. Lukas, W. Liu, K. Esfarjani, C. Opeil, D. Broido, G. Chen, and Z. Ren, Proceedings of the National Academy of Sciences **110**, 13261 (2013).
[10] O. Delaire, J. Ma, K. Marty, A. F. May, M. A. McGuire, M.-H. Du, D. J. Singh, A. Podlesnyak, G. Ehlers, M. D. Lumsden, and B. C. Sales, Nature Materials **8**, 614 (2011).
[11] K. M. O. Jensen, E. S. Božin, C. D. Malliakas, M. B. Stone, M. D. Lumsden, M. G. Kanatzidis, S. M. Shapiro, and S. J. L. Billinge, Physical Review B **86**, 085313 (2012).
[12] J. An, A. Subedi, and D. J. Singh, Solid State Communications **148**, 417 (2008).
[13] Y. Zhang, X. Ke, P. R. C. Kent, J. Yang, and C. Chen, Physical Review Letters **107**, 175503 (2011).
[14] T. Shiga, J. Shiomi, J. Ma, O. Delaire, T. Radzynski, A. Lusakowski, K. Esfarjani, and G. Chen, Physical Review B **85**, 155203 (2012).
[15] Z. Tian, J. Garg, K. Esfarjani, T. Shiga, J. Shiomi, and G. Chen, Physical Review B **85**, 184303 (2012).
[16] S. Lee, K. Esfarjani, T. Luo, J. Zhou, Z. Tian, and G. Chen, Nature Communications **5**, 3525 (2014).
[17] T. F. Smith, J. A. Birch, and J. G. Collins, Journal of Physics C: Solid State Physics **9**, 4375 (2001).
[18] G. Lucovsky and R. M. White, Physical Review B **8**, 660 (1973).
[19] P. B. Littlewood, Journal of Physics C: Solid State Physics **13**, 4855 (1980).
[20] P. B. Littlewood, Journal of Physics C: Solid State Physics **13**, 4875 (1980).
[21] A. Bussmann-Holder, H. Bilz, and P. Vogl, *Electronic and Dynamical Properties of IV-Vl Compounds*, Springer Tracts in Modern Physics, Vol. 99 (Springer, 1983) pp. 1–48.
[22] K. M. Rabe and J. D. Joannopoulos, Physical Review B **32**, 2302 (1985).
[23] H. A. Alperin, S. J. Pickart, J. J. Rhyne, and V. J. Minkiewicz, Physics Letters A **40**, 295 (1972).
[24] W. Jantsch, Springer Tracts in Modern Physics, Vol. 99 (Springer-Verlag, 1983).
[25] P. Brüesch, *Phonons: Theory and Experiments* (Springer-Verlag, 1982).
[26] G. P. Srivastava, *The physics of phonons* (Taylor and Francis, 1990).
[27] B. Fultz, Progress in Materials Science **55**, 247 (2010).
[28] W. Cochran, Advances in Physics **9**, 387 (1960).
[29] G. S. Pawley, W. Cochran, R. A. Cowley, and G. Dolling, Physical Review Letters **17**, 753 (1966).
[30] S. Kastbjerg, N. Bindzus, M. Søndergaard, S. Johnsen, N. Lock, M. Christensen, M. Takata, M. A. Spackman, and B. B. Iversen, Advanced Functional Materials **23**, 5477 (2013).
[31] T. Shiga, T. Murakami, T. Hori, O. Delaire, and J. Shiomi, Applied Physics Express **7**, 041801 (2014).
[32] F. Bridges, T. Keiber, S. Medling, and B. C. Sales, Physica Status Solidi C **10**, 236 (2013).
[33] T. Keiber, F. Bridges, and B. C. Sales, Physical Review Letters **111**, 095504 (2013).
[34] K. S. Knight, Journal of Physics: Condensed Matter **26**, 385403 (2014).
[35] S. W. Lovesey, *Theory of Neutron Scattering from Condensed Matter*, Vol. 1 (Clarendon, 1984).
[36] H. Burkhard, G. Bauer, and A. Lopez-Otero, Journal of the Optical Society of America **67**, 943 (1977).
[37] C. W. Li, O. Hellman, J. Ma, A. F. May, H. B. Cao, X. Chen, A. D. Christianson, G. Ehlers, D. J. Singh, B. C. Sales, and O. Delaire, Physical Review Letters **112**, 175501 (2014).
[38] Y. Chen, X. Ai, and C. A. Marianetti, Physical Review Letters **113**, 105501 (2014).
[39] E. I. Rogacheva, G. V. Gorne, N. K. Zhigareva, and A. B. Ivanova, Inorganic Materials **27**, 194 (1991).
[40] M. Iizumi, Y. Hamaguchi, K. F. Komatsubara, and Y. Kato, Journal of the Physical Society of Japan **38**, 443 (1975).
[41] T. Seddon, S. C. Gupta, and G. A. Saunders, Solid State Communications **20**, 69 (1976).
[42] C. W. Li, O. Hellman, J. Ma, A. F. May, H. B. Cao, X. Chen, A. D. Christianson, G. Ehlers, D. J. Singh, B. C. Sales, and O. Delaire, Physical Review Letters **112**, 175501, EPAPS (2014).
[43] K. L. I. Kobayashi, Y. Kato, Y. Katayama, and K. F. Komatsubara, Physical Review Letters **37**, 772 (1976).

[44] D. L. Abernathy, M. B. Stone, M. J. Loguillo, M. S. Lucas, O. Delaire, X. Tang, J. Y. Y. Lin, and B. Fultz, Review of Scientific Instruments **83**, 015114 (2012).
[45] J. Taylor and et al., Bulletin of the American Physical Society **57** (2012).
[46] M. Kresch, O. Delaire, R. Stevens, J. Y. Y. Lin, and B. Fultz, Physical Review B **75**, 104301 (2007).
[47] J. Rodríguez-Carvajal, Physica B: Condensed Matter **192**, 55 (1993).
[48] G. Ehlers, A. A. Podlesnyak, J. L. Niedziela, E. B. Iverson, and P. E. Sokol, Review of Scientific Instruments **82**, (2011).
[49] T. G. Perring, R. A. Ewings, and J. V. H. Duijn, http://horace.isis.rl.ac.uk (2009).
[50] http://www.neutron.ethz.ch/research/resources/reslib.
[51] E. R. Cowley, J. K. Darby, and G. S. Pawley, Journal of Physics C: Solid State Physics **2**, 1916 (1969).
[52] N. Gillis, Physical Review Letters **22**, 1251 (1969).
[53] D. Strauch and R. Becher, Journal of Physics C: Solid State Physics **20**, 1641 (1987).
[54] G. Kresse and J. Furthmüller, Computational Materials Science **6**, 15 (1996).
[55] G. Kresse and J. J. Hafner, Physical Review B **47**, 558 (1993).
[56] G. Kresse and J. Furthmüller, Physical Review B **54**, 11169 (1996).
[57] O. Hellman, P. Steneteg, I. A. Abrikosov, and S. I. Simak, Physical Review B **87**, 104111 (2013).
[58] G. Squires, *Introduction to the theory of thermal neutron scattering* (Cambridge University Press, 1978).
[59] P. Bauer Pereira, I. Sergueev, S. Gorsse, J. Dadda, E. Müller, and R. P. Hermann, Physica Status Solidi B (2012).
[60] W. Keune, Physical Review B **10**, 5057 (1974).
[61] O. Hellman and I. A. Abrikosov, Physical Review B **88**, 144301 (2013).